Hindawi
Shock and Vibration
Volume 2020, Article ID 6637282, 15 pages
https://doi.org/10.1155/2020/6637282

Research Article

A Modified Asymmetric Bouc–Wen Model-Based Decoupling Control of an XY Piezoactuated Compliant Platform with Coupled Hysteresis Characteristics

Xubin Zhou,[1,2] Weidong Chen,[1] Qing Xiao,[3] Xiangsen Kong,[2] Xingtian Liu,[2] Liping Zhou,[2] Yichong Dong,[3] and Quan Zhang[3]

[1]*Academy of Astronautics, Nanjing University of Aeronautics and Astronautics, Nanjing 210016, China*
[2]*Shanghai Satellite Engineering Institute, Shanghai 201108, China*
[3]*School of Mechatronic Engineering and Automation, Shanghai University, Shanghai 200072, China*

Correspondence should be addressed to Quan Zhang; lincolnquan@shu.edu.cn

Received 4 October 2020; Revised 30 November 2020; Accepted 6 December 2020; Published 16 December 2020

Academic Editor: Yong Zhu

Due to the inherent hysteresis characteristics of the smart material, the positioning accuracy of the piezo-driven manipulator was always decreased. Especially in multi-degrees-of-freedom (MDOFs) compliant manipulators driven by multismart actuators, the cross-coupled hysteresis among MDOFs decreased the positioning accuracy of such compliant platforms significantly. In this paper, the hysteresis feature identification and coupled hysteresis compensation of a piezo-driven XY manipulator was investigated. To establish the hysteresis characteristics of the piezo-driven manipulator, a modified Bouc–Wen model has been proposed, and a Genetic Algorithm-based Particle Swarm Optimization (GA-PSO) was adopted to recognize the parameters of the model. To improve the output performances of the manipulator, the decoupling controller of the XY micromanipulator was designed, and the driven voltages were modified using the estimated coupling displacements. The experiments validated that the modified Bouc–Wen model featured the ability to present the hysteresis process effectively, and the maximum prediction errors are 0.19 μm and 0.16 μm in the two directions separately. The coupled hysteresis displacement before and after implementing the decoupling controller in the X-direction was reduced from 0.56 μm to 0.15 μm, and the coupling effect is reduced by 73.2%, while in the Y-direction, the coupling effect was also decreased by 72.9%.

1. Introduction

Precision positioning manipulator was an important technology in advanced manufacturing field, which was widely used in aerospace, weapons, semiconductor manufacturing, and medical microscopy [1–3]. Piezoelectric actuators (PZT actuators), as the smart-material-based actuators, featured the characteristics of fast response, low power consumption, and high positioning resolution [4] and, hence, were commonly adopted in the manipulator with high positioning accuracy [5, 6]. However, the nonlinear characteristics which existed in piezoelectric actuators [7] caused by hysteresis and creep decreased the positioning accuracy of the corresponding compliant manipulators. Especially for manipulators with MDOFs, the mutual interference among multiple piezoelectric actuators resulted in a coupled hysteresis effect, which further degraded the positioning accuracy of the manipulator and even caused the system to deviate from the equilibrium state. Therefore, to compensate the coupled hysteresis effects, the decoupling controller [8] of the piezo-driven compliant platform was usually designed using the identified hysteresis model to improve the output performances of the platform.

Many models had been used to present the nonlinearity of the piezoelectric actuator. To describe the hysteresis features founded in PZT actuators, Wang et al.[9] developed an improved Preisach model, and the results demonstrated that the derived model keeps a bias with the real hysteresis

curves. In order to investigate the effect of the rate dependence features, Liang [10] proposed an improved Prandtl–Ishlinskii (PI) model to update the recoil operator according to the input rate, which effectively increased the precision of the proposed model. Another commonly used model was the Bouc–Wen model [11–13], which could describe most of the hysteresis characteristics by only changing several model parameters. In [14], an asymmetry item was integrated into the classical model, forming a modified Bouc–Wen model featuring the asymmetric hysteresis description ability. Wang et al.[15] developed an asymmetric Bouc–Wen model, and the experimental results showed that such model can effectively describe the asymmetric hysteresis curve with less tracking error compared to the classical Bouc–Wen model. Based on the intelligent algorithm of GA-PSO, the inverse compensation control for a piezoelectric actuator using a modified Bouc–Wen model was conducted in [16]. Moreover, the model parameters identification was also the key issue to enhance the hysteresis modelling ability, which will further increase the inverse compensation precision of the manipulator. Therefore, a GA-PSO algorithm with strong global search ability and high efficiency was adopted in this study to recognize the model parameters. Zhang et al.[17] adopted a GA method to identify the parameters of the proposed model of a lithium ion battery, and the simulation data were consistent with the experimental data. Such intelligent algorithms were also wildly applied in many other mechanical systems [18, 19]. Otherwise, the numerical simulation algorithms were also significant before the experiments [20–22].

The hysteresis coupling effect referred to the mutual interference among several smart actuators with the hysteresis features in different directions. Taking the decoupled XY piezo-driven compliant manipulator as an example, ideally, the two directions of the platform were orthogonal, and there was no mutual influence in the two directions theoretically. However, due to the manufacturing and design error, the decoupled mechanical structure could hardly achieve the totally decoupled feature. Hence, the hysteresis coupling effects among multiple DOFs were caused, leading the positioning precision of the manipulator to decrease greatly, especially under the nanolevel positioning precision. Another significant reason was that the presented decoupled XY compliant manipulators were usually designed with the particular mechanical structures to achieve the independent DOF, such as the symmetric parallel four-bar mechanism, which made the manipulator not belong to the complete decoupled mechanism such as the serial mechanism. Nowadays, some decoupling controllers based on nonlinear coupling models have been developed [23–25]. Among them, a hybrid control approach using to compensate the interacted hysteresis between two different DOFs while tracking the reference trajectory was developed by Wang and Tang.[26]. In [27], the force-displacement relationship of the stage was analyzed using a motion control mathematical model, and the analytical models for displacement and cross-coupling error in the XY-directions were derived. In addition, Habineza et al.[28] developed a nonlinear controller based on the differential geometry decoupling theory to control an eddy current damper, and the proposed approach was validated to have the ability to realize the motion in horizontal and vertical directions. In this study, to decrease the effect caused by the coupled hysteresis, a feedforward decoupling controller was adopted using the identified inverse Bouc–Wen model, and such approach features the advantages of low cost and no changing of the structure of the initial platform. Since the coupling hysteresis effect in the piezo-driven manipulator was a complex nonlinear phenomenon, it was a challenging work to design the decoupling controller with multiactuators. Therefore, the model identification and the decoupling controller design of the compliant manipulator with MDOFs were required to be further studied.

The rest of the paper is arranged as follows: An improved asymmetric Bouc–Wen model featuring the hysteresis description ability is developed in Section 2. Then, in Section 3, a modified GA algorithm optimized by PSO is established. A decoupling control approach using the identified Bouc–Wen model has been investigated to reduce the coupling hysteresis effect of the XY piezo-driven manipulator in Section 4. Then, the experiments are conducted, and the results are discussed in Section 5. At last, Section 6 gives the conclusion of the paper.

2. The Modified Asymmetric Bouc–Wen Model

The Bouc–Wen model owned the ability to establish the complicated hysteresis characteristics with relatively fewer parameters. It can identify the hysteresis model based on the displacement data acquired by the experiment. Figure 1 shows the hysteresis model established by the Bouc–Wen model, and the corresponding expression is given as follows [29]:

$$F(x,z) = \alpha k \cdot x + (1-\alpha)k \cdot z, \tag{1}$$

$$\dot{z} = A \cdot \dot{x} - \beta \cdot |\dot{x}| \cdot |z|^{n-1} \cdot z - \gamma \cdot \dot{x} \cdot |z|^{n}, \tag{2}$$

where the specific definition of the parameters can be found in [16].

The conventional Bouc–Wen expression usually describes a symmetric hysteresis loop, as shown in Figure 1(a), and in practice, the piezoelectric actuator usually exhibits asymmetric hysteresis features. Hence, the conventional Bouc–Wen expression was required to be modified to describe the features of asymmetric hysteresis. Thus, by introducing an asymmetrical item to equations (1) and (2), the new expression of equation (2) is shown as follows:

$$\begin{cases} \dot{h}(t) = A \cdot \dot{u}(t) - \beta \cdot |\dot{u}(t)| \cdot |h(t)|^{n-1} \\ \cdot h(t) - \gamma \cdot \dot{u}(t) \cdot |h(t)|^{n} + \Delta\varepsilon, \\ \Delta\varepsilon = \delta u(t) \cdot \operatorname{sgn}(\dot{u}(t)). \end{cases} \tag{3}$$

Combined equations (1) and (3), the description of an independent hysteresis curve can be simplified as follows:

$$y_{\mathrm{bw}}(t) = H[\cdot] = p \cdot u(t) + q \cdot h(t), \tag{4}$$

where $H[\cdot]$ is the hysteresis model, A, β, γ, and n can be identified by the data acquired through the experiments, and

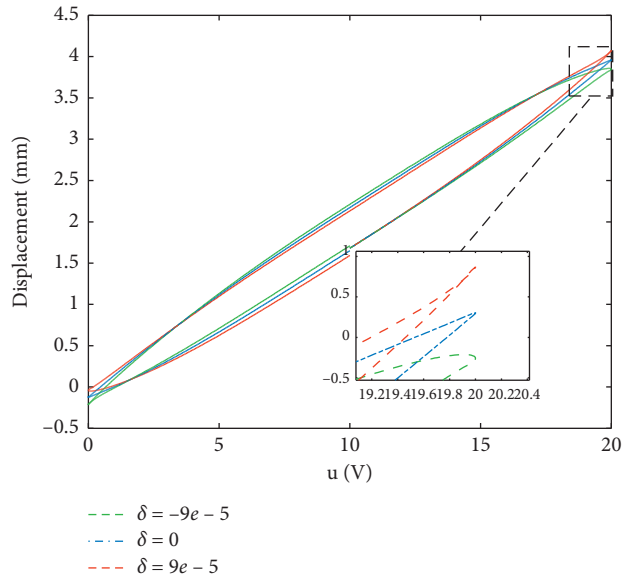

Figure 1: Asymmetric hysteresis curves with different δ.

δ is the added asymmetric hysteresis item. As observed in Figure 1, with the variation of variable δ, the shape of the hysteresis curve changed to different asymmetric curves.

3. The Intelligent GA-PSO Approach

When the hysteresis model was established, all the parameters of the model were initial values which required to be further identified based on the experimental data. In this paper, a GA-PSO approach featuring both the advantages of GA and PSO was adopted to implement the parameter recognition. The particle swarm optimization algorithm can solve a large number of nonlinear and noncontinuous problems and was widely used in science and engineering. Genetic algorithm was a global optimization algorithm using the effective optimization of genetic principles. Combining the advantages of PSO and GA algorithms, the GA-PSO algorithm adopted in this paper had a faster convergence speed and global search ability. The procedure of the adopted GA-PSO algorithm is illustrated in Figure 2.

Usually, the exact solution of the Bouc–Wen model is unknown, and whether the identified parameter was a global optimal solution or not was required to be estimated. Therefore, the only criterion for judging whether the recognized result was suitable was the coincidence extent between the model results and the test data. The fitness function is presented as follows:

$$F(p, q, A, \beta, \gamma, n, \delta) = \sqrt{\frac{1}{L}\sum_{i=1}^{L}(y - y_{\mathrm{bw}})^2}, \quad (5)$$

where the specific definition of the parameters in equation (5) can be found in our previous research [16].

4. Decoupling Control of the XY Piezoelectric Positioning Platform

Before designing the decoupling controller, the linearization method used to reduce the hysteresis effect in independent direction without considering the coupled effects was required first. According to Wang et al. and Habineza et al. [11, 28], the feedforward compensation control methods are adopted, and the hysteresis compensation controller for an independent direction was developed. Combined with formula (4), its inverse model expression is

$$v(t) = H^{-1}[\cdot] = \frac{1}{p}y_r - q\,h(t), \quad (6)$$

where y_r is the reference displacement for the input, $v(t)$ is the required drive voltage, and $H^{-1}[\cdot]$ is the inverse model in the X-direction. The compensation principle is shown in Figure 3.

In order to realize the hysteresis compensation control in the X- and Y-direction, combined with the feedforward compensation control principle, the feedforward compensation controller shown in Figure 4 was designed in Simulink. The controller was divided into four areas: signal input, hysteresis inverse model parameters, hysteresis, and feedforward control.

In the ideal state of the positioning platform, as shown in Figure 5, the X-direction and Y-direction of the decoupled XY manipulator should be orthogonal and have no coupling effect. However, influenced by the hysteresis of the piezoelectric actuator, the parallel structure, and assembly errors of the actuators, the hysteresis coupling effects between the X- and Y-direction were found to exist.

When a sinusoidal signal with the amplitude of 5 V and frequency of 2 Hz was applied in the Y-direction and the

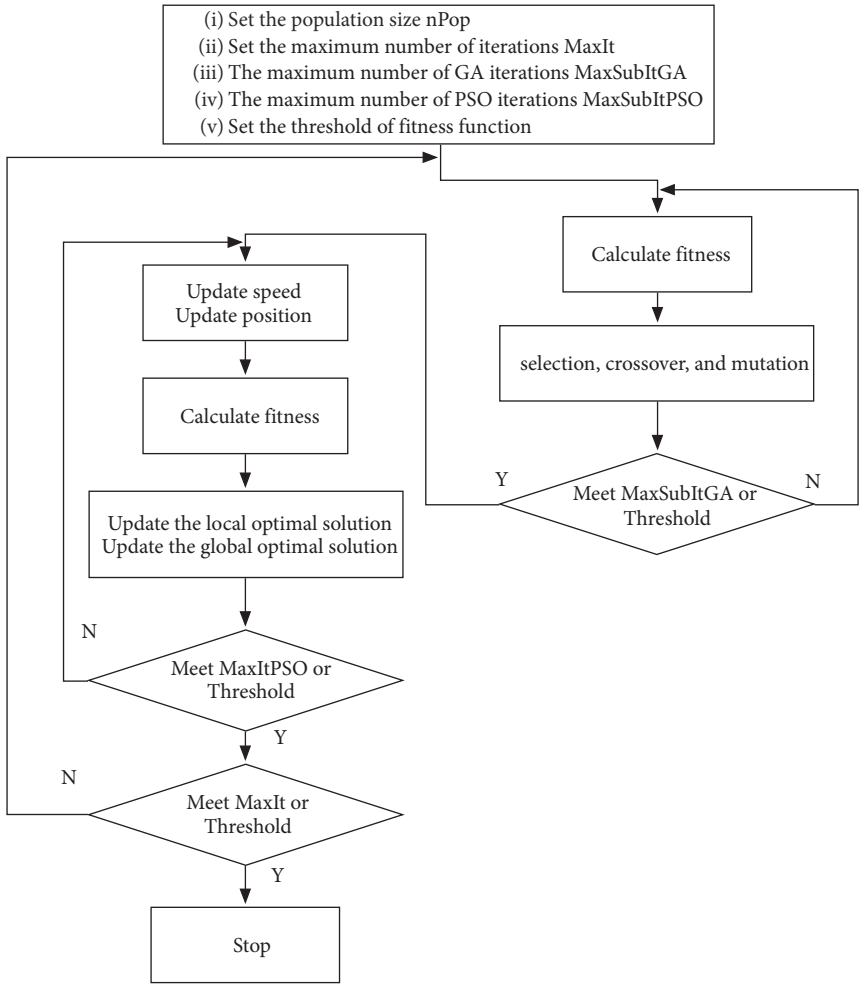

Figure 2: The procedure of the adopted GA-PSO algorithm.

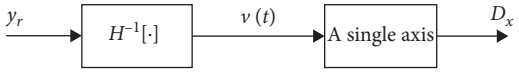

Figure 3: The principle of the feedforward compensation control.

signal of 0 V was applied in the X-direction respectively, the output displacement in the X-direction should be zero if all the conditions were ideal. However, the coupling displacement of in the X-direction caused by the coupled effects was measured, as shown in Figure 6(a). Figure 6(b) shows the measured hysteresis curve in the Y-direction. It can be observed in Figure 6(a) that the output displacement in the X-direction was also a hysteresis curve, which further validated the coupled hysteresis characteristic between the X- and Y-direction. Similar results can be obtained by exchanging the excited voltage. Figure 6(c) presents the output displacement in the Y-direction when a sinusoidal signal with an amplitude of 5 V and a frequency of 2 Hz was applied in the X-direction and the input voltage 0 V was applied in the Y-direction, respectively. The coupling hysteresis output characteristic had also been observed. Figure 6(d) presents the measured hysteresis curve in the X-direction. These results further verify the fact that, in a piezo-driven manipulator with MDOFs, the output displacement in one direction was not only affected by the hysteresis from its driven actuator but also suffered the coupled hysteresis effect from other actuators.

Based on the proposed asymmetric Bouc–Wen model which can present the coupling process of the platform, a decoupling controller was further designed to reduce both the independent hysteresis and coupled hysteresis effect of the XY platform. The basic principle of the decoupling control was to calculate the displacement in the X-direction which is caused by the excitation from the Y-direction, and then, the displacement caused by the coupling hysteresis effect was compensated by applying an opposite driving voltage in the X-direction. The relationship between the input voltage and the output displacement is defined as follows:

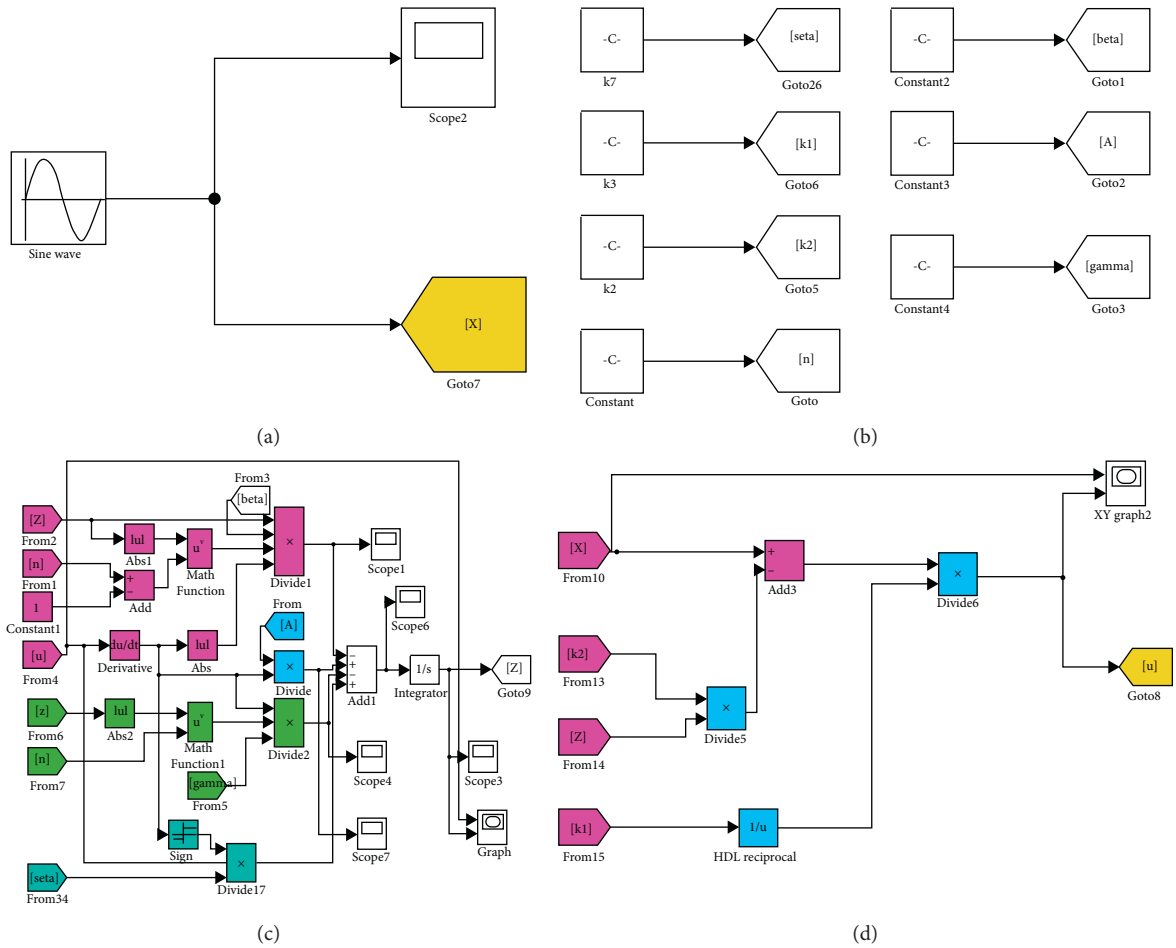

Figure 4: Feedforward controller. (a) Signal input. (b) Model parameter. (c) Hysteresis. (d) Feedforward control.

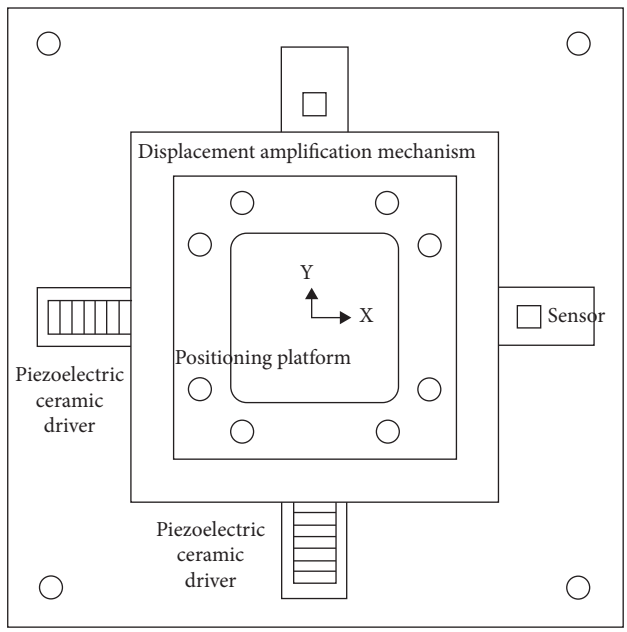

Figure 5: Schematic diagram of the XY piezoactuated compliant platform.

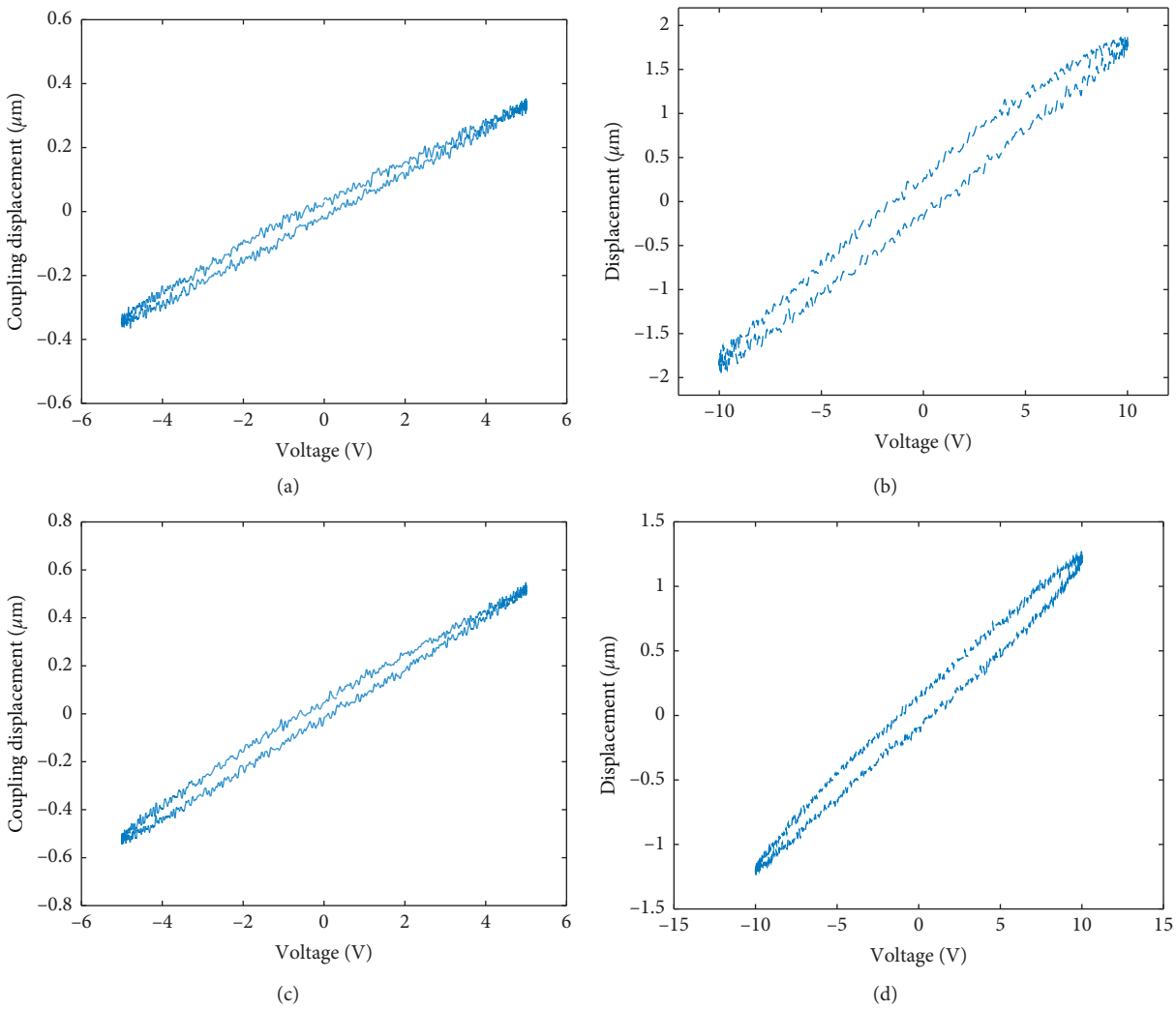

Figure 6: Hysteresis coupling between the X- and Y-direction. (a) Coupling Hysteresis in the X-direction. (b) Hysteresis displacement in the Y-direction. (c) Coupling hysteresis in the Y-direction. (d) Hysteresis displacement in the X-direction.

$$\begin{bmatrix} D_x(t) \\ D_y(t) \end{bmatrix} = H \begin{bmatrix} v_x(t) \\ v_y(t) \end{bmatrix}, \tag{7}$$

where $v_x(t)$ and $v_y(t)$ represent the driving voltages in the X- and Y-direction, $D_x(t)$ and $D_y(t)$ represent the output displacements of the platform in the X- and Y-direction, respectively, and $H[\cdot]$ is the hysteresis mathematical model of the platform.

The control methods of the manipulator in the two directions are the same. When only considering the output displacement in the X-direction, the coupled model in the X-direction should satisfy the following relation:

$$D_x(t) = H_{XX}[v_x(t)] + H_{XY}[v_y(t)], \tag{8}$$

where $H_{xx}[\cdot]$ is a hysteresis model between the input voltage $v_x(t)$ and the output displacement $D_x(t)$ in the X-direction and $H_{xy}[\cdot]$ represents an effect model between the input voltage in the Y-direction and displacement in the X-direction caused by the decoupling effect.

Based on the decoupling control principle and formula (8), the decoupling control model is

$$D_x(t) = H_{XX}[v_x(t) + v_{xy}(t)] + H_{XY}[v_y(t)], \tag{9}$$

$$v_{xy}(t) = H_{XX}^{-1} H_{XY}[v_y(t)], \tag{10}$$

where H_{xx}^{-1} is the inverse model of the hysteresis in the X-direction, $v_{xy}(t)$ is the driving voltage for compensating the coupling effect in the X-direction, and $H_{xy}[v_y(t)]$ is a coupling displacement in the X-direction caused by the voltage $v_y(t)$ applied in the Y-direction.

We combined formula (9) with the feedforward compensation formula (6) and replaced the driving voltage $v_x(t)$ in the X-direction and the coupling compensation control voltage $v_{xy}(t)$ in formula (9) with the reference displacements $u_x(t)$ and $u_{xy}(t)$:

$$D_x(t) = H_{XX}H_{XX}^{-1}\left[u_x(t) + u_{xy}(t)\right] + H_{XY}\left[v_y(t)\right]. \quad (11)$$

According to the feedforward control principle, $v_y(t)$ can be obtained by combining formula (6):

$$v_y(t) = H_{YY}^{-1}\left[u_y(t)\right]. \quad (12)$$

According to formula (9), the required coupling compensation reference displacement $u_{xy}(t)$ is

$$u_{xy}(t) = D_x(t) - H_{XX}\left[v_x(t) + v_{xy}(t)\right]. \quad (13)$$

The decoupling controller in the Y-direction is the same with that derived in the X-direction, and the decoupling control model in the Y-direction can be obtained:

$$D_y(t) = H_{YY}H_{YY}^{-1}\left[u_y(t) + u_{yx}(t)\right] + H_{YX}\left[v_x(t)\right], \quad (14)$$

$$u_{yx}(t) = D_y(t) - H_{YY}\left[v_y(t) + v_{yx}(t)\right], \quad (15)$$

$$v_x(t) = H_{XX}^{-1}\left[u_x(t)\right]. \quad (16)$$

The working principles of the decoupling controller of the two-dimensional piezoelectric positioning platform can be obtained by formulas (11) and (14), as shown in Figure 6. Despite for the compensate voltage computed from the independent hysteresis effect in the actuation direction, the decoupling controller in the X-direction also calculated the compensate displacement caused by the voltage applied in the Y-direction through the coupling model. The compensate displacement can be calculated by the inverse hysteresis model of the piezoelectric actuator in X-direction. Then, the compensate voltage computed from the coupled displacement was combined with the original control voltage to form the final drive voltage in the X-direction.

According to the abovementioned decoupling control principle, combined with the design of the feedforward control method, the decoupling controller in Figure 7 was established in Simulink, as shown in Figure 8. The decoupling controller in the Y-direction was the same as the design in the X-direction.

5. Experimental Verification

5.1. Experimental Setup. In order to verify the performance of the decoupling controller, a test system was designed based on the XY200S piezoelectric positioning table (Harbin Core Tomorrow Co., Ltd). The stroke of the platform in the X-direction was 144.37 μm, and the stroke in the Y-direction was 149.27 μm. The entire platform is fixed on an isolation platform to reduce the environmental vibration. The output of the XY piezo-driven platform is tested using a laser interferometer. The experimental setup is shown in Figure 9.

5.2. Inverse Compensation Control without Hysteresis Coupling. Firstly, independent feedforward inverse compensation control experiments were performed on the output of the platform in one direction without considering the influence of hysteresis coupling. The input voltage in the Y-direction is set as 0 V, a sinusoidal signal with a frequency of 2 Hz and a magnitude of 10 V is applied in the X-direction, and then, the output displacement is measured in the X-direction. The GA-PSO was used to identify the hysteresis model in the X-direction based on the experimental data, and the feedforward inverse decoupling compensation controller was used based on formula (6) to verify the compensation ability. The experimental method in the Y-direction was the same as that derived in the X-direction; the input voltage in the X-direction is set as 0 V, a sinusoidal signal with a frequency of 2 Hz and a magnitude of 10 V is applied in the Y-direction, and then, the output displacement is collected in the Y-direction. The parameter identification results of the hysteresis model in the X- and Y-direction are shown in Table 1.

Figures 10(a) and 10(b) show the comparison between the identified asymmetric Bouc–Wen model and the experimental acquisition displacement in the X-direction. Figure 10(c) demonstrates the displacement error tracked between the identified model and the actual acquired data, and the tracking error range was −0.19 μm to 0.11 μm in the X-direction, which verified the predicting precision of the identified model.

Figures 11(a) and 11(b) show the comparison of the asymmetric Bouc–Wen hysteresis model in the Y-direction with the experimental acquisition displacement after the model parameters were identified. Figure 11(c) presents the displacement error tracked between the model and the actual acquired data, and the tracking error range in the Y-direction was calculated to be −0.09 μm to 0.16 μm.

According to result in Figures 10 and 11, the identified model can effectively describe the hysteresis nonlinearity in the X- and Y-direction. Then, the parameter identification results in Table 1 were, respectively, substituted to the feedforward compensation controller shown in Figure 4 for the feedforward compensation control experiment. After the feedforward compensation control, the compensation results, as shown in Figures 12 and 13, were obtained, and the hysteresis phenomenon in two directions of the piezoelectric positioning platform was obviously improved.

The maximum linearity error of the feedforward control based on the Bouc–Wen hysteresis model is defined as

$$\Delta\max_e = \max\left|d_e - d\right|, \quad (17)$$

where d_e is the displacement of the output in one direction after the feedforward compensation control and d is the ideal displacement in one direction.

The nonlinearity calculation formula is defined as

$$\eta = \frac{\Delta\max_e}{d_t}, \quad (18)$$

where d_t is the maximum output displacement of the output in one direction after the feedforward compensation control.

When the amplitude of the reference displacement input in the X-direction was 1.25 μm and the sinusoidal signal was 2 Hz, the maximum linear error in the X-direction was calculated as 0.10 μm, and the nonlinearity was 8%; when the

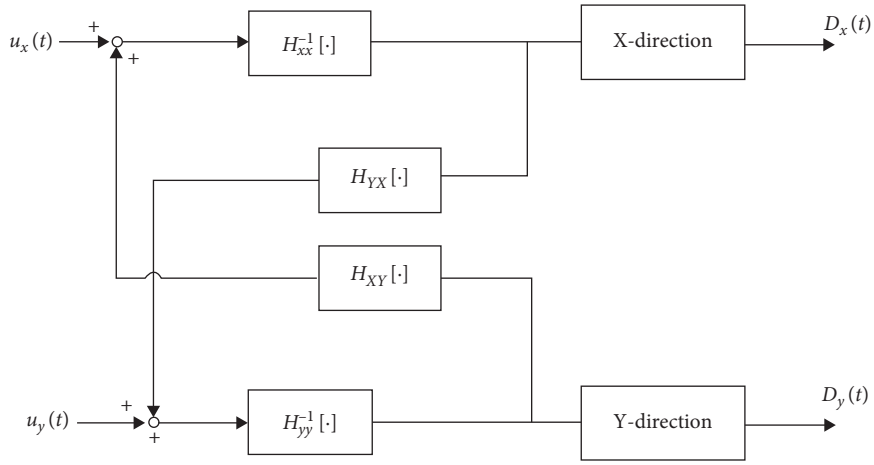

FIGURE 7: Block diagram of the coupled hysteresis compensation based on the decoupling control system for an XY compliant manipulator.

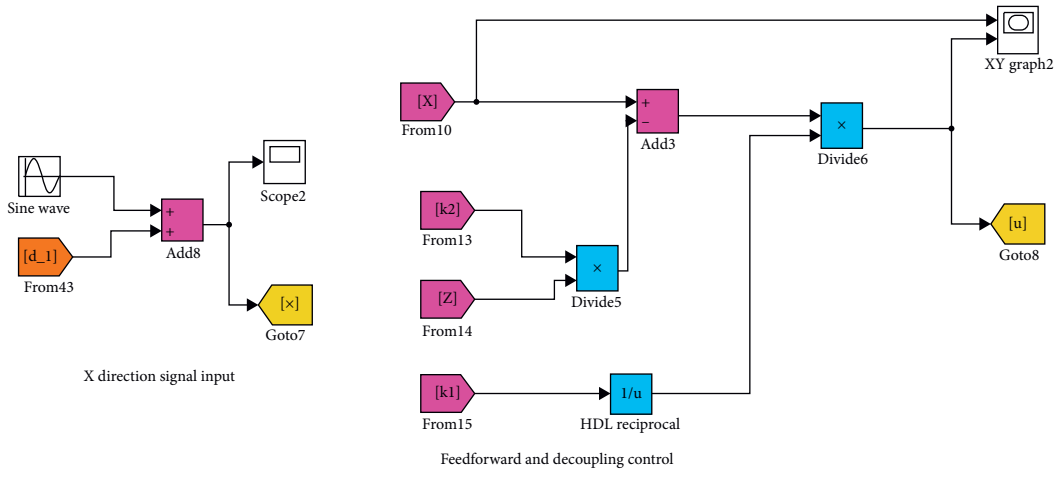

(a)

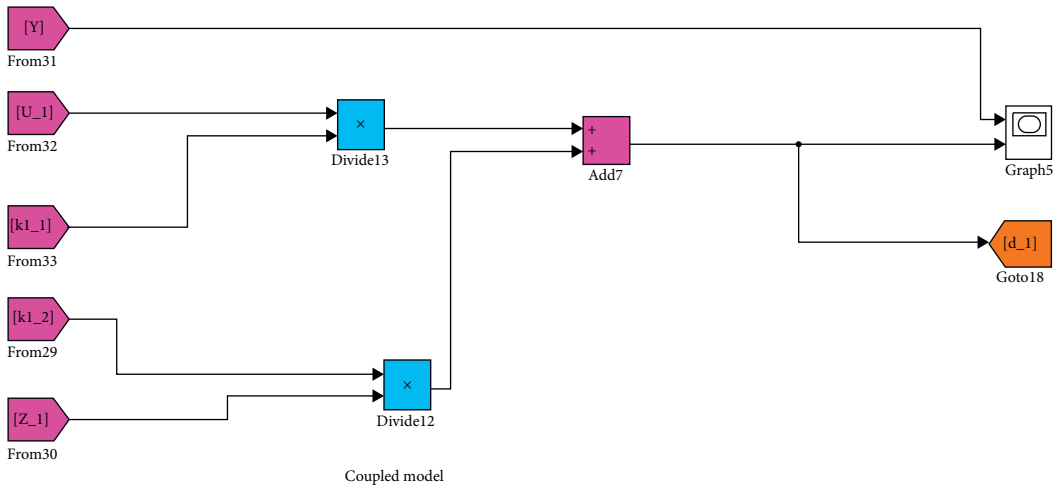

(b)

FIGURE 8: Continued.

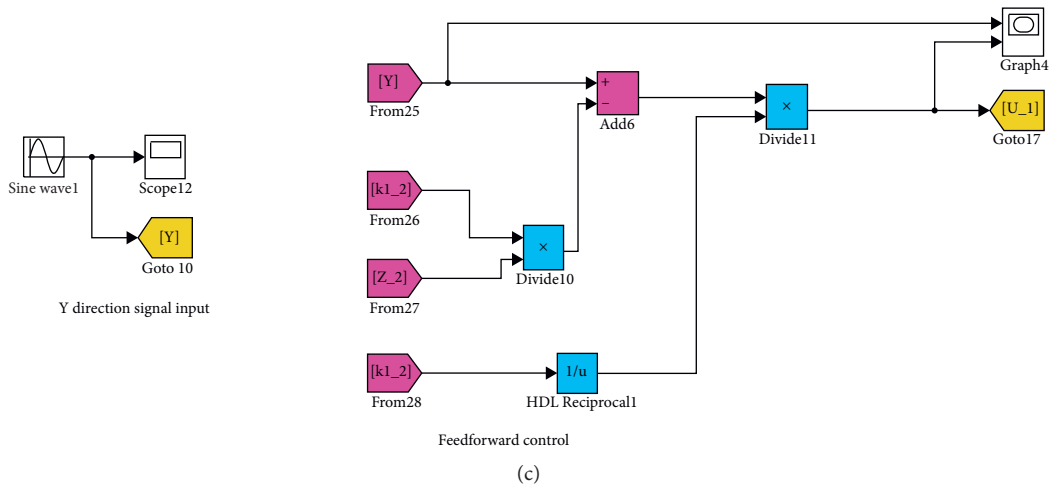

(c)

Figure 8: Decoupling control design in the X-direction. (a) Decoupling control in the X-direction. (b) The coupling model from the Y-direction. (c) The corresponding control voltage from the Y-direction (input signal of the coupled model).

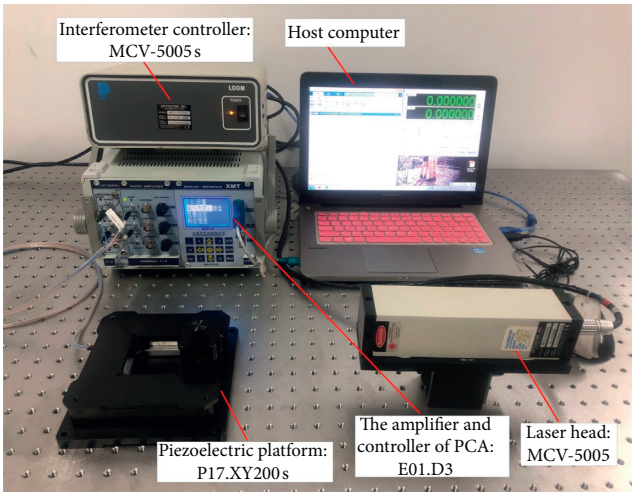

Figure 9: Experimental setup.

Table 1: Parameter identification results of the hysteresis model in the X- and Y-direction.

Parameter	H_{XX}	H_{YY}
p	8.70969×10^{-4}	2.13628×10^{-4}
q	−1.67281	−0.707036
A	4.5108×10^{-4}	8.93308×10^{-5}
β	17.354	8.7715
γ	3.6121	−0.523075
n	2.5	1.5
δ	−0.003487	1.423×10^{-3}

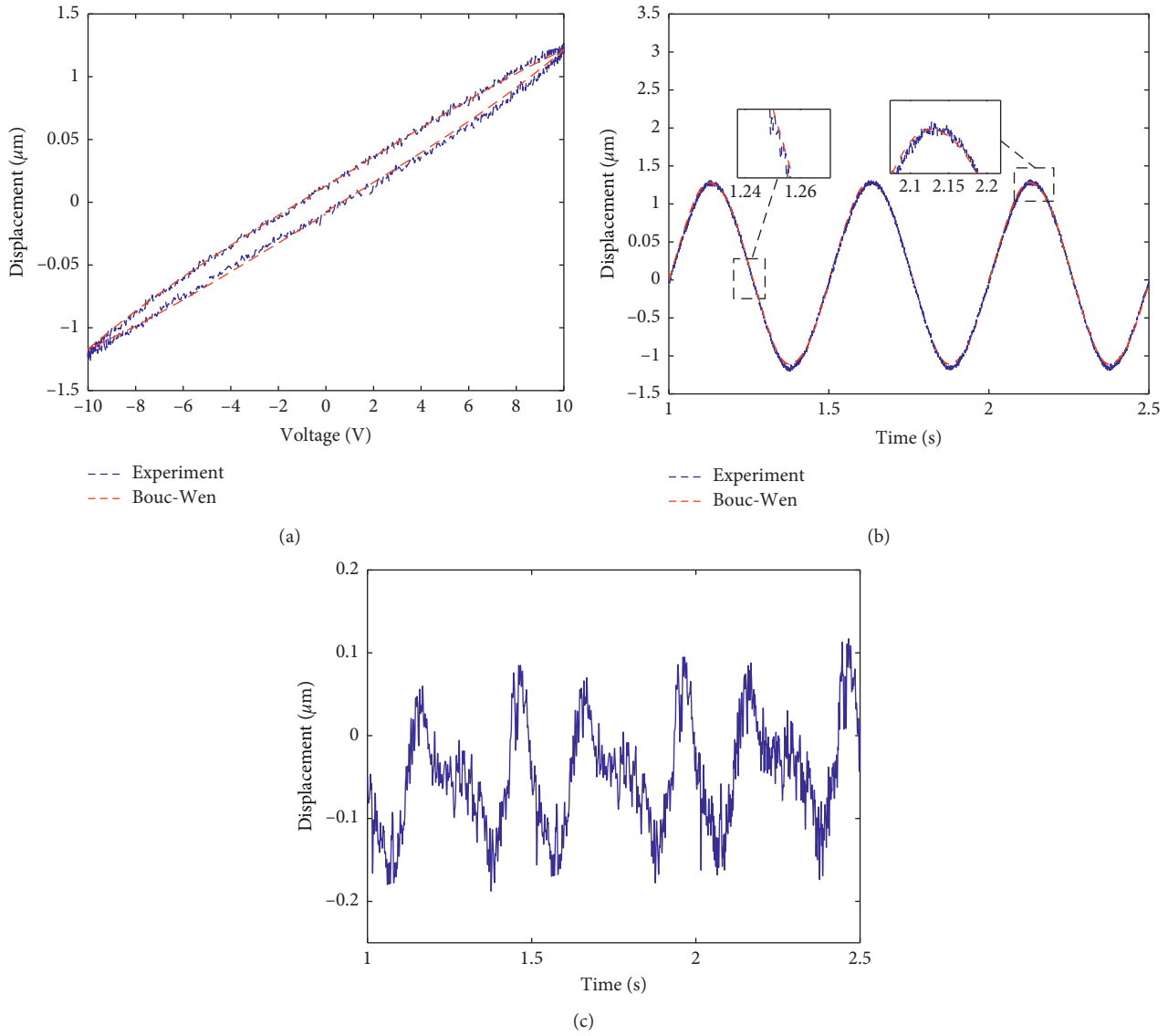

Figure 10: X-direction identification results. (a) Comparison between the hysteresis model and the experimental data. (b) Displacement tracking of the hysteresis model. (c) Tracking error in the X-direction.

reference displacement was 2 μm and the frequency was 2 Hz, the maximum linearity error in the Y-direction was 0.11 μm and the nonlinearity was 5.5%.

5.3. Hysteresis Decoupling Control. Taking the decoupling control in the X-direction as the example, the coupling model was established using the proposed modified Bouc–Wen model with the parameters recognized by the GA-PSO approach. The coupling model was developed to estimate the offset resulted from the Y-direction. The coupling voltage was applied in the X-direction to achieve the purpose of decoupling control in the X-direction.

The key to decoupling control was to establish a coupling model. According to the coupled displacement data in Figure 5, the GA-PSO algorithm was adopted to recognize the coupled model in the X- and Y-direction through the modified Bouc–Wen model. Table 2 shows the parameters in the coupled model in the X- and Y-direction, namely, the H_{XY} and H_{YX} in formulas (8) and (11). Combined with the designed feedforward compensation controller, the decoupling controller in the X-direction was designed in Simulink, as shown in Figure 13(a) , and the decoupling controller design method in the Y-direction was the same as the design procedure in the X-direction.

Decoupling experiments were performed to verify the effectiveness. In the Y-direction, a sinusoidal signal with amplitude of 2 μm and a frequency of 2 Hz was set as the input signal. When the input of the X-direction is 0 V, the amplitude of the coupled displacement in the X-direction was 0.56 μm before the decoupling control, and the displacement error was reduced to 0.15 μm after the decoupling control, as shown in Figure 14. The coupling effect in the X-direction is reduced by 73.2%. Figure 15 shows a sinusoidal

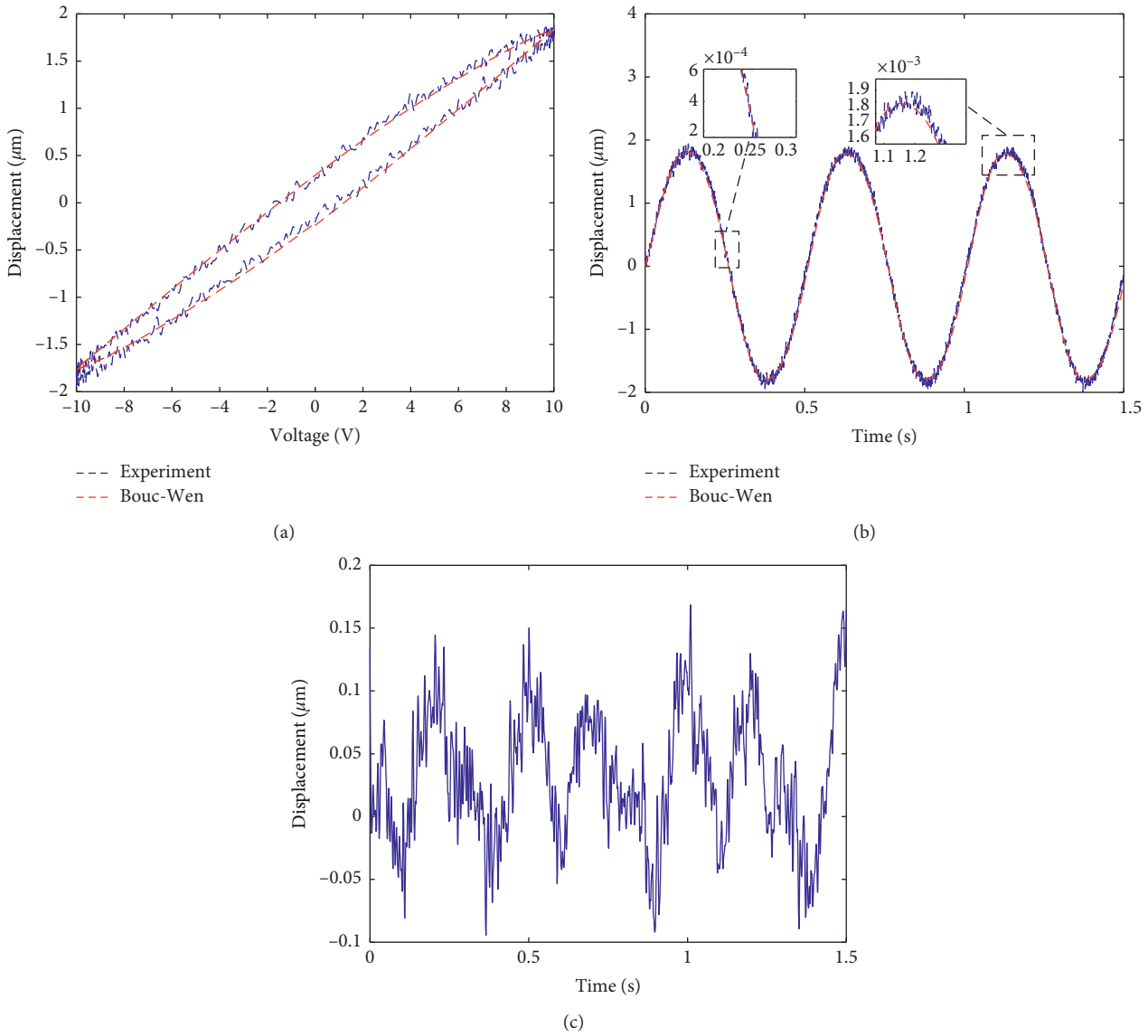

Figure 11: Y-direction identification results. (a) Comparison between the hysteresis model and the experimental data. (b) Displacement tracking of the hysteresis model. (c) Tracking error in the Y-direction.

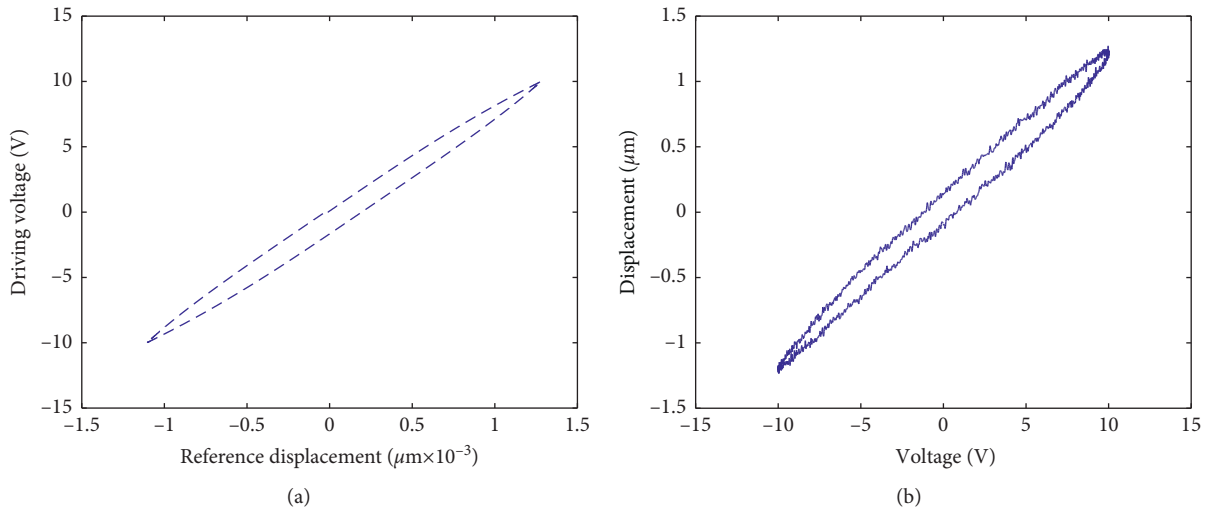

Figure 12: Continued.

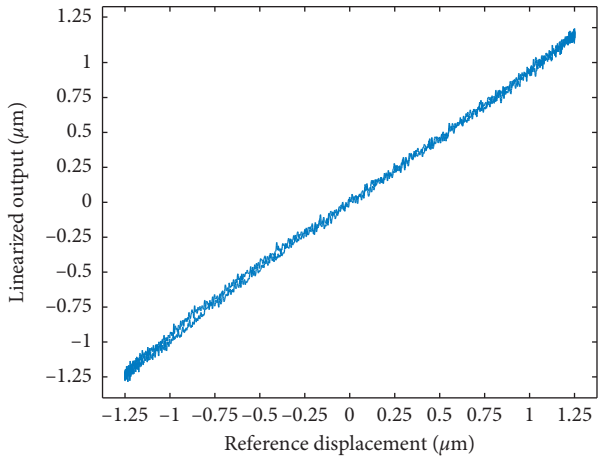

(c)

FIGURE 12: The feedforward compensation results in the X-direction. (a) The hysteresis inverse model in the X-direction. (b) The output hysteresis curve. (c) The linearized output.

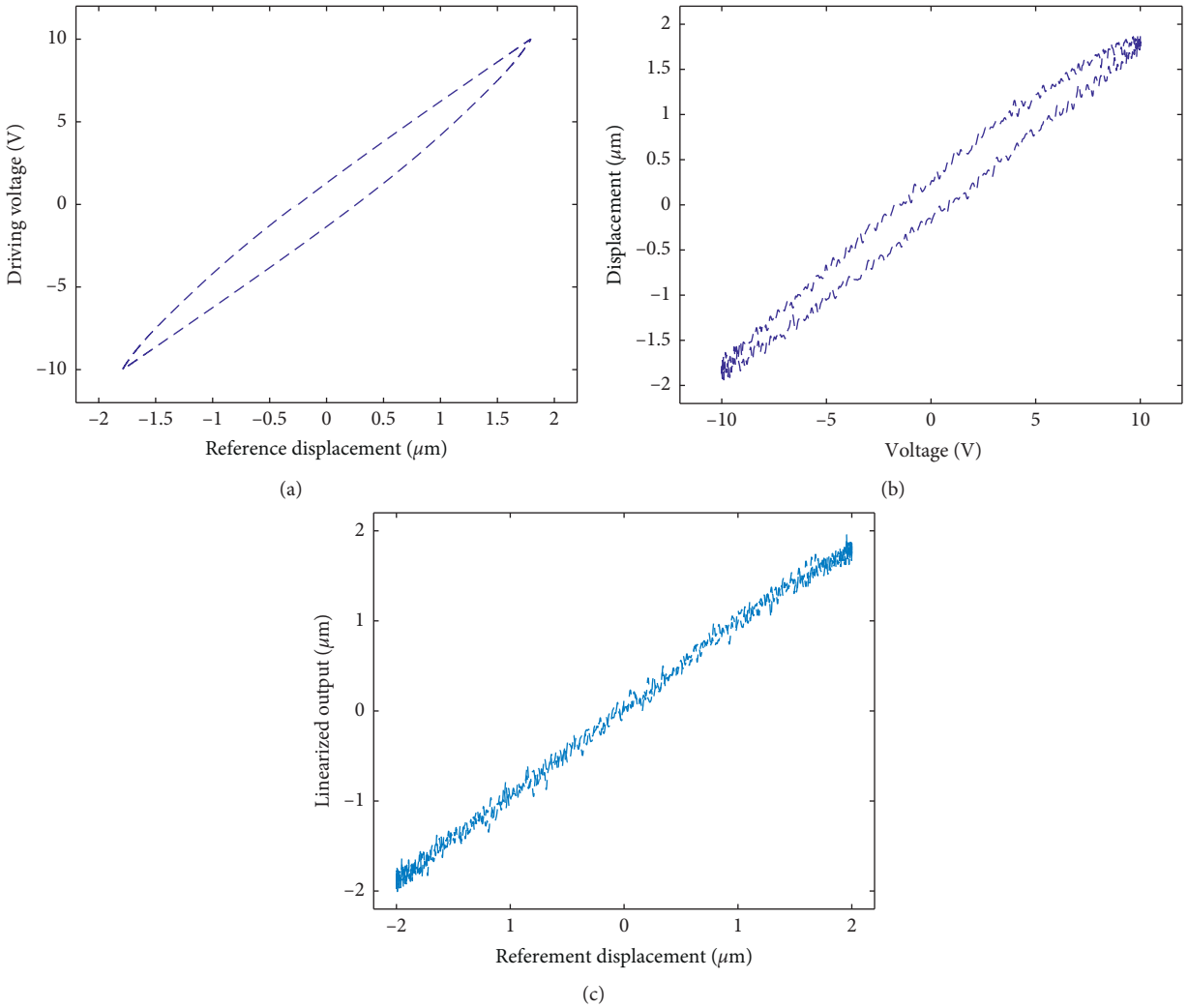

(a) (b)

(c)

FIGURE 13: The feedforward compensation results in the Y-direction. (a) The hysteresis inverse model in the Y-direction. (b) The output hysteresis curve. (c) The linearized output.

Table 2: Parameter identification results of coupling models in the X- and Y-direction.

Parameter	H_{XY}	H_{YX}
p	2.03378×10^{-5}	5.15847×10^{-5}
q	2.38428×10^{-3}	0.0255589
A	0.04192	0.00182372
β	10.7864	19.1426
γ	1.80684	4.23868
n	1.9	1.8
δ	−0.00983677	0.00047382

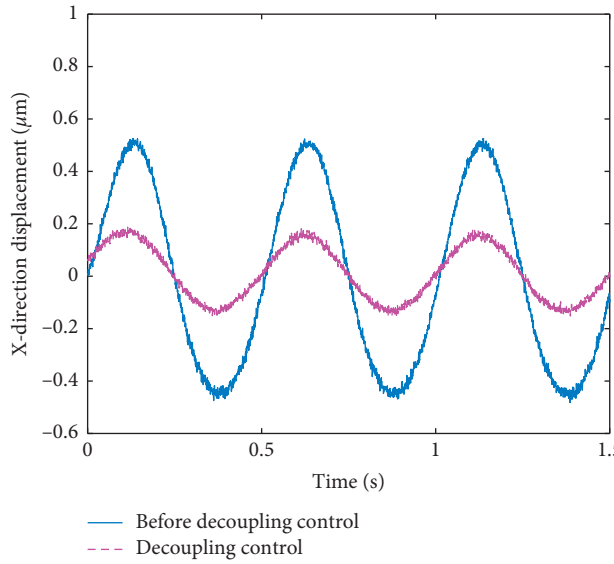

Figure 14: Decoupling control in the X-direction.

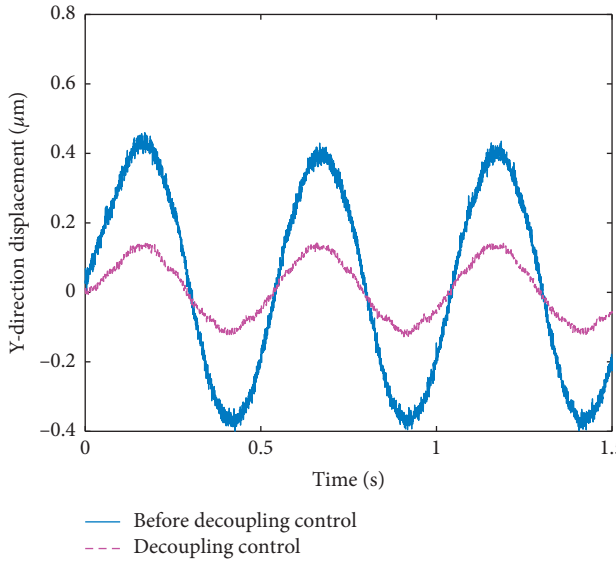

Figure 15: Decoupling control in the Y-direction.

signal with amplitude of 2 μm and a frequency of 2 Hz in the X-direction. When the input in the Y-direction was 0 v, the displacement before and after the decoupling control in the Y-direction was measured. The amplitude of the coupling displacement in the Y-direction was 0.48 μm before the decoupling control, and the displacement error is decreased to 0.13 μm after the decoupling control. The coupling effect in the Y-direction was decreased by 72.9%. Due to the

limitation of the experimental setup, a special case of the decoupling experiment was conducted to validate the effectiveness of the proposed method.

6. Conclusions

In this paper, an improved Bouc–Wen model featuring the ability to depict the hysteresis characteristics of an XY micromanipulator was investigated. The inverse hysteresis model was developed in order to design the decoupling controller of the XY micromanipulator, and the model parameters were identified based on a GA-PSO algorithm. Experiments showed that the proposed Bouc–Wen can effectively track the hysteresis characteristics. The hysteresis coupling effect of the platform was reduced efficiently with the application of the designed decoupling controller. The coupling displacement amplitude in the X-direction was decreased from 0.56 μm to 0.15 μm, and the coupling effect was reduced by 73.2% during the experiment. The coupling displacement amplitude in the Y-direction was decreased from 0.48 μm to 0.13 μm, and the coupling effect was reduced by 72.9%.The results validated that the proposed identification and decoupling control approaches owned the ability to counteract the coupling hysteresis effect of the piezo-driven manipulator with MDOFs, and the positioning precision of the MDOFs piezo-driven manipulator can be improved without changing the initial structure of the manipulator.

Data Availability

The data used to support the findings of this study are available from the corresponding author upon request.

Conflicts of Interest

The authors declare that they have no conflicts of interest.

Acknowledgments

This work was supported by the National Natural Science Foundation of China under Grant nos. 61973207, 51875363, and 51605271, Shanghai Rising-Star Program under Grant no. 20QA1403900, the Natural Science Foundation of Shanghai under Grant no. 19ZR1474000, and the State Key Laboratory of Mechanics and Control of Mechanical Structures (Nanjing University of Aeronautics and Astronautics, Grant no. MCMS-E-0320G01).

References

[1] S. Akbari and T. Pirbodaghi, "Precision positioning using a novel six axes compliant nano-manipulator," *Microsystem Technologies*, vol. 23, no. 7, pp. 1–9, 2016.

[2] Q. Zhang, J. K. Mills, W. L. Cleghorn, J. Jin, and C. Zhao, "Trajectory tracking and vibration suppression of a 3-PRR parallel manipulator with flexible links," *Multibody System Dynamics*, vol. 33, no. 1, pp. 27–60, 2015.

[3] Q. Zhang, J. Zhao, Y. Peng, H. Pu, and Y. Yang, "A novel amplification ratio model of a decoupled XY precision positioning stage combined with elastic beam theory and Castigliano's second theorem considering the exact loading force," *Mechanical Systems and Signal Processing*, vol. 136, Article ID 106473, 2020.

[4] A. Safa, R. Y. Abdolmalaki, S. Shafiee, and B. Sadeghi, "Adaptive nonsingular terminal sliding mode controller for micro/nanopositioning systems driven by linear piezoelectric ceramic motors," *ISA Transactions*, vol. 77, pp. 122–132, 2018.

[5] Q. Zhang, C. Li, J. Zhang, and X. Zhang, "Synchronized motion control and precision positioning compensation of a 3-DOFs macro-micro parallel manipulator fully actuated by piezoelectric actuators," *Smart Materials and Structures*, vol. 26, no. 11, Article ID 115001, 2017.

[6] Q. Zhang, C. Li, J. Zhang, and J. Zhang, "Smooth adaptive sliding mode vibration control of a flexible parallel manipulator with multiple smart linkages in modal space," *Journal of Sound and Vibration*, vol. 411, pp. 1–19, 2017.

[7] Y. Guo and Y. Zhu, "Modeling and analysis on hysteresis nonlinear characteristics of the piezoelectric stack actuators [J]," *Piezoelectrics & Acoustooptics*, vol. 39, no. 4, pp. 520–524, 2017.

[8] H. E. Jing-Feng, W. J. Xie, and J. W. Han, "Output decoupling control of 6-DOF parallel manipulator," *Journal of Harbin Institute of Technology*, vol. 38, no. 3, pp. 395–398, 2006.

[9] W. Wang, W. Guo, and D. Liu, "Neural network hysteresis modeling with an improved Preisach model for piezoelectric actuators," *Engineering Computations*, vol. 29, no. 3, pp. 248–259, 2012.

[10] C. Liang, F. Wang, Y. Tian, X. Zhao, and D. Zhang, "Grasping force hysteresis compensation of a piezoelectric-actuated wire clamp with a modified inverse Prandtl-Ishlinskii model," *Review of Scientific Instruments*, vol. 88, no. 11, Article ID 115101, 2017.

[11] D. Wang, S. Yan, and Z. Wei, "Bouc-Wen model based feedforward linearization controller for piezoceramic microactuators," *Chinese Journal of Scientific Instrument*, vol. 36, no. 7, pp. 1514–1521, 2015.

[12] L. J. Zhao, D. U. Yong-Feng, H. Wang et al., "Nonlinear characteristics identification of rubber isolation bearing base on Bouc-Wen model," *Journal of Lanzhou University of Technology*, vol. 43, no. 1, pp. 116–121, 2017.

[13] M. Gan, Z. Qiao, and Y. Li, "Sliding mode control with perturbation estimation and hysteresis compensator based on bouc-wen model in tackling fast-varying sinusoidal position control of a piezoelectric actuator," *Journal of Systems Science and Complexity*, vol. 29, no. 2, pp. 367–381, 2016.

[14] W. Zhu and D.-h. Wang, "Non-symmetrical Bouc-Wen model for piezoelectric ceramic actuators," *Sensors and Actuators A: Physical*, vol. 181, no. 1, pp. 51–60, 2012.

[15] G. Wang, G. Chen, and F. Bai, "Modeling and identification of asymmetric Bouc-Wen hysteresis for piezoelectric actuator via a novel differential evolution algorithm," *Sensors and Actuators A: Physical*, vol. 235, pp. 105–118, 2015.

[16] Q. Zhang, Y. Dong, Y. Peng, J. Luo, S. Xie, and H. Pu, "Asymmetric Bouc-Wen hysteresis modeling and inverse compensation for piezoelectric actuator via a genetic algorithm-based particle swarm optimization identification algorithm," *Journal of Intelligent Material Systems and Structures*, vol. 30, no. 8, pp. 1263–1275, 2019.

[17] L. Zhang, L. Wang, G. Hinds, C. Lyu, J. Zheng, and J. Li, "Multi-objective optimization of lithium-ion battery model using genetic algorithm approach," *Journal of Power Sources*, vol. 270, no. 3, pp. 367–378, 2014.

[18] S. Tang, S. Yuan, and Y. Zhu, "Deep learning-based intelligent fault diagnosis methods toward rotating machinery," *IEEE Access*, vol. 8, no. 1, pp. 9335–9346, 2020.
[19] S. Tang, S. Yuan, and Y. Zhu, "Convolutional neural network in intelligent fault diagnosis toward rotatory machinery," *IEEE Access*, vol. 8, no. 1, pp. 86510–86519, 2020.
[20] Y. Yang, L. Zhou, W. Shi, Z. He, Y. Han, and Y. Xiao, "Interstage difference of pressure pulsation in a three-stage electrical submersible pump," *Journal of Petroleum Science and Engineering*, vol. 196, Article ID 107653, 2020.
[21] L. Zhou, C. Han, L. Bai, W. Li, M. A. El-Emam, and W. Shi, "CFD-DEM bidirectional coupling simulation and experimental investigation of particle ejections and energy conversion in a spouted bed," *Energy*, vol. 211, Article ID 118672, 2020.
[22] H. Yan, X. Su, H. Zhang et al., "Design approach and hydrodynamic characteristics of a novel bionic airfoil," *Ocean Engineering*, vol. 216, Article ID 108076, 2020.
[23] B. A. M. Owens and B. P. Mann, "Linear and nonlinear electromagnetic coupling models in vibration-based energy harvesting," *Journal of Sound and Vibration*, vol. 331, no. 4, pp. 922–937, 2012.
[24] N. G. Ulu, E. Ulu, and M. Cakmakci, "Learning Based Cross-Coupled Control for Multi-Axis High Precision Positioning Systems," *Legged Locomotion*, vol. 2, 2012.
[25] N. G. Ulu, E. Ulu, and M. Cakmakci, "Design and analysis of a modular learning based cross-coupled control algorithm for multi-axis precision positioning systems," *International Journal of Control, Automation and Systems*, vol. 14, no. 1, pp. 272–281, 2016.
[26] H. Wang and L. Tang, "Modeling and experiment of bistable two-degree-of-freedom energy harvester with magnetic coupling," *Mechanical Systems and Signal Processing*, vol. 86, pp. 29–39, 2017.
[27] W. M. Wang, S. Y. Ma, W. Q. Wang, and C. L. Dian, "Nonlinear control of maglev positioning stage," in *proceedings of the Sixth International Symposium on Precision Engineering Measurements and Instrumentation*, vol. 7544, p. 75441H, International Society for Optics and Photonics, Hangzhou, China, August 2010.
[28] D. Habineza, M. Rakotondrabe, and Y. Le Gorrec, "Bouc-wen modeling and feedforward control of multivariable hysteresis in piezoelectric systems: application to a 3-DoF piezotube scanner," *IEEE Transactions on Control Systems Technology*, vol. 23, no. 5, pp. 1797–1806, 2015.
[29] F. Ikhouane, J. E. Hurtado, and J. Rodellar, "Variation of the hysteresis loop with the Bouc-Wen model parameters," *Nonlinear Dynamics*, vol. 48, no. 4, pp. 361–380, 2007.